Structure-Borne Noise Transmission into Cylindrical Enclosures of Finite Extent

Dimitri A. Bofilios*
Integrated Aerospace Sciences Corporation (INASCO), Athens, Greece
and
Constantinos S. Lyrintzis†
San Diego State University, San Diego, California 92182

This paper presents an analytical study of structure-borne noise transmission of finite, double-wall-laminated, fiber-reinforced cylindrical enclosures due to stochastic excitations. The stochastic excitations are either uniform random pressures or random point loads with specified spectral densities. The theoretical solutions of the governing acoustic-structural equations are obtained via modal decomposition and a Galerkin-like approach. Numerical results indicative of the effects of acoustic and structural variations are offered.

Introduction

THE design of many transportation structures is impacted by the interaction of functional requirements such as strength, stiffness, weight, passenger comfort, cargo containment, reliability, etc. To accommodate many of these requirements, new design concepts for lower weight and reduced cost are needed. Composite materials could provide weight and structural integrity advantages.[1-4] However, the low-weight composites do not seem to provide any advantage over conventional materials such as aluminum with respect to noise attenuation.[5] Past studies have demonstrated that sandwich constructions can achieve a significant amount of response and noise reduction.[6-11] To satisfy the required vibroacoustic environment, the designs from composite materials might need to be modified to include the double-wall sandwich concepts.

This paper presents an analytical study of structure-borne noise of double-wall-laminated, closed, circular cylindrical shells. Structural response and noise in the inteior are obtained by using modal expansions and a Galerkin-like procedure.[10,11] The inputs are uniformly distributed random pressure and random point forces. The shell skins are modeled according to a laminated cylindrical thin shell theory.[12-17] The end caps are taken as double-wall circular isotropic plates.[18-20] The governing differential equations for the vibration of double-wall shells and double-wall circular plates shown in Figs. 1 and 2 are developed for the case in which the core material is taken to be very soft, so that bending and shearing stresses can be neglected, and, consequently, the core can be described by a uniaxial constitutive law. Such a core model allows in-phase (flexural) and out-of-phase (dilatational) motions of the double-wall system.[10,11] The solutions for the acoustic pressure in the shell interior are obtained in terms of the inner shell and/or the inner circular plate motions. Hard wall and absorbent boundary conditions are considered.

The paper contains numerical results of sound pressure levels in the cylindrical enclosure due to vibrations of homogeneous isotropic (aluminum) and laminated fiber-reinforced composite double-wall shells. Results of noise transmission through double-wall circular plates are also presented. It is shown that, by proper selection of the dynamic parameters, damping characteristics, and fiber orientation, the noise in the interior can be reduced.

Received Jan. 18, 1990; revision received May 23, 1990; accepted for publication July 24, 1990.

*Technical Director, Department of Research and Development, 22 Miaouli Street, Moschato 18345.

†Associate Professor, Department of Aerospace Engineering and Engineering Mechanics. Member AIAA.

Analytical Model

Acoustic Solution

Consider a closed cylindrical enclosure with volume $V = \pi R^2 L$ shown in Fig. 1. The geometrical parameters of the enclosure are defined in detail in Fig. 1. It is assumed that the walls of the multilayered cylindrical shell and the circular end plates are flexible. However, the motions of the shell and the end plates are taken to be independent. Thus, the acoustic pressure inside the enclosure can be obtained from

$$p = p_1 + p_2 \tag{1}$$

where p_1 and p_2 are the acoustic pressure due to inner shell and inner plate motions, respectively. The pressure p inside the

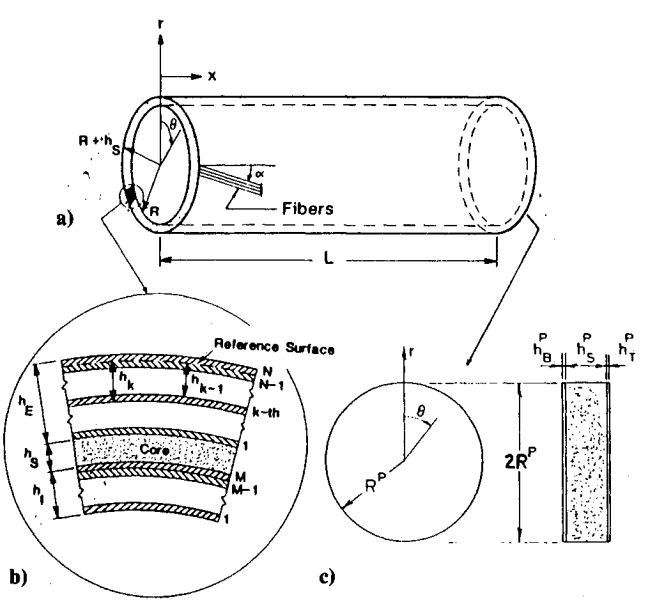

Fig. 1 Problem geometry: a) geometry of double-wall-laminated composite shell; b) shell structure; c) double-wall circular plate.

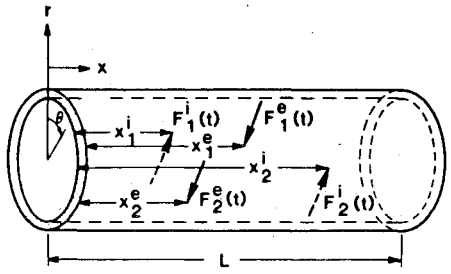

Fig. 2 Distribution of random loads acting on the shell.

enclosure satisfies the wave equation in cylindrical polar coordinates,[21-23]

$$\nabla^2 p - \beta \dot{p} = \ddot{p}/c^2 \tag{2}$$

in which β and c are the acoustic damping and speed of sound in the cavity, respectively; a dot indicates time derivative; and

$$\nabla^2 = \frac{\partial}{\partial r^2} + \frac{1}{r}\frac{\partial}{\partial r} + \frac{1}{r^2}\frac{\partial^2}{\partial^2 \theta} + \frac{\partial^2}{\partial x^2} \tag{3}$$

The interior walls at $r = R$ and $x = 0$, L are taken to be absorbent with a prescribed point impedance[24] $Z(\omega)$. The boundary conditions to be satisfied are

$$\frac{\partial p_1}{\partial r} = -\rho \ddot{w}_B(x,\theta,t) - \frac{\rho}{Z_A}\dot{p}_1 \quad \text{at} \quad r = R \tag{4}$$

$$\frac{\partial p_1}{\partial x} = 0 \quad \text{at} \quad x = 0, L \tag{5}$$

$$\frac{\partial p_2}{\partial x} = \rho \ddot{w}_1(r,\theta,t) + \frac{\rho}{Z_1}\dot{p}_2 \quad \text{at} \quad x = 0 \tag{6}$$

$$\frac{\partial p_2}{\partial x} = -\rho \ddot{w}_2(r,\theta,t) - \frac{\rho}{Z_2}\dot{p}_2 \quad \text{at} \quad x = L \tag{7}$$

$$\frac{\partial p_2}{\partial r} = 0 \quad \text{at} \quad r = R \tag{8}$$

where ρ is the air density; Z_A, Z_1, and Z_2 are the absorbent wall impedances; and w_B, w_1, and w_2 are displacements in the normal direction (positive outward) of the inner shell and the inner end plates, respectively. Taking the Fourier transformation of Eqs. (2-8) and writing the solution in terms of the orthogonal acoustic modes corresponding to acoustically hard walls yields

$$\bar{p}_1(x,r,\theta,\omega) = \sum_{i=0}^{\infty}\sum_{j=0}^{\infty} P_{ij}(r,\omega)X_{ij}(x,\theta) \tag{9}$$

$$\bar{p}_2(x,r,\theta,\omega) = \sum_{k=0}^{\infty}\sum_{j=1}^{\infty} Q_{kj}(x,\omega)Y_{kj}(r,\theta) \tag{10}$$

where the acoustic modes for a closed cylindrical enclosure are

$$X_{ij} = \sqrt{\frac{2}{\pi L}}\cos(i\pi x/L)\cos(j\theta) \tag{11}$$

$$Y_{kj} = J_k(\lambda_{kj} r)\cos(k\theta) \tag{12}$$

where J_k represents the Bessel function of the first kind of order k, and $\lambda_{kj} = \tilde{\alpha}_{kj}/R$, where $\tilde{\alpha}_{kj}$ is the jth root of the equation $dJ_k/dr = 0$. Equation (11) is obtained by solving the wave equation where the end plates are assumed to be rigid boundaries without acoustic energy dissipation, and the only source of acoustic energy is the boundary at $r = R$. Similarly, Eq. (12) represents the solution to the wave equation, where the acoustic source is at $x = 0$ or $x = L$, and there is no acoustic energy dissipation at $r = R$. Substituting Eqs. (9) and (10) into Eq. (2) and using orthogonality condition of acoustic modes, one obtains

$$\frac{d^2 P_{ij}}{dr^2} + \frac{1}{r}\frac{dP_{ij}}{dr} + (\sigma_i^2 - j^2/r^2)P_{ij} = 0 \tag{13}$$

$$\frac{d^2 Q_{kj}}{dx^2} + \gamma_{kj}^2 Q_{kj} = 0 \tag{14}$$

in which

$$\sigma_i^2 = (\omega/c)^2 - (i\pi/L)^2 - \underline{i}\omega\beta \tag{15}$$

$$\gamma_{kj}^2 = (\omega/c)^2 - \lambda_{kj}^2 - \underline{i}\omega\beta \tag{16}$$

and $\underline{i} = \sqrt{-1}$. Solving Eqs. (13) and (14) and imposing the finiteness condition of the pressure $\bar{p}_1$ at $r = 0$ gives

$$\bar{p}_1(x,r,\theta,\omega) = \sum_{i=0}^{\infty}\sum_{j=0}^{\infty}\alpha_{ij}J_j(\sigma_i r)X_{ij}(x,\theta) \quad \text{for} \quad \sigma_i^2 > 0 \tag{17}$$

$$\bar{p}_2(x,r,\theta,\omega) = \sum_{k=0}^{\infty}\sum_{j=1}^{\infty}\Big[A_{kj}\sin(\gamma_{kj}x) + B_{kj}\cos(\gamma_{kj}x)\Big]Y_{kj}(r,\theta) \tag{18}$$

in which α_{ij}, A_{kj}, and B_{kj} are arbitrary constants. For $\sigma_i^2 < 0$ the Bessel function J_j needs to be replaced with the modified Bessel function I_j in Eq. (17). For the special case when $\sigma_i^2 = 0$ the solution for the pressure p_1 is

$$\bar{p}_1(x,r,\theta,\omega) = \sum_{i=0}^{\infty}\sum_{j=0}^{\infty} C_{ij} r^j X_{ij}(x,\theta) \tag{19}$$

where C_{ij} are arbitrary constants, and r^j are the solutions for P_{ij} obtained by the Frobenius method from Eq. (13) when $\sigma_i^2 = 0$. Using the boundary conditions specified in Eqs. (4-8) and expanding the shell, w_B, and the end plate, w_1, w_2, motions in terms of the appropriate modal eigenfunctions one obtains

$$\bar{p}_1(x,r,\theta,\omega) = \rho\omega^2\sum_{i=0}^{\infty}\sum_{j=0}^{\infty}\Big[e_{ij}G_{ij}(r,\omega)\sum_{m=1}^{\infty}\sum_{n=0}^{\infty}\bar{A}_{mn}^B L_{mnij}\Big]X_{ij}(x,\theta) \tag{20}$$

$$\bar{p}_2(x,r,\theta,\omega) = \sum_{k=0}^{\infty}\sum_{j=1}^{\infty}\frac{\epsilon_{kj}}{\Delta_{kj}}\sum_{s=0}^{\infty}\sum_{q=1}^{\infty}\{[(e_{kj}^{(1)} - \underline{i}e_{kj}^{(2)}/Z_1)\times \bar{A}_{sq}^L L_{sqkj}^L + (\underline{i}\rho^2\omega^3/Z_2)\bar{A}_{sq}^R L_{sqkj}^R]\sin(\gamma_{kj}x) + [\rho\omega^2\gamma_{kj}\bar{A}_{sq}^R L_{sqkj}^R + (e_{kj}^{(3)} + \underline{i}e_{kj}^{(4)}/Z_1)\bar{A}_{sq}^L L_{sqkj}^L]\times\cos(\gamma_{kj}x)\}J_k(\lambda_{kj}r)\cos k\theta \tag{21}$$

where

$$e_{ij} = \begin{cases} 1/4 & \text{if} \quad i = 0, \quad j = 0 \\ 1/2 & \text{if} \quad i \neq 0, \quad j = 0; \quad i = 0, \quad j \neq 0 \\ 1 & \text{if} \quad i \neq 0, \quad j \neq 0 \end{cases} \tag{22}$$

$$G_{ij} = \begin{cases} r^j/\Big[jR^{j-1} + \underline{i}\omega\rho R^j/Z_A\Big] & \text{for} \quad \sigma_i = 0 \\ J_j(\sigma_i r)/\Big[\sigma_i J_j'(\sigma_i R) + \underline{i}\omega\rho J_j(\sigma_i R)/Z_A\Big] & \text{for} \quad \sigma_i > 0 \end{cases} \tag{23}$$

$$L_{mnij} = \int_0^L\int_0^{2\pi} X_{mn}^s(x,\theta)X_{ij}(x,\theta) \tag{24}$$

$$\epsilon_{kj} = \frac{1}{\int_0^{R^p} \int_0^{2\pi} r J_k^2(\lambda_{kj} r) \cos^2(k\theta)\, dr\, d\theta}; \quad R^p \le R + h_s \tag{25}$$

$$\Delta_{kj} = i\rho\omega\gamma_{kj} \cos(\gamma_{kj}L)(1/Z_1 + 1/Z_2) - \sin(\gamma_{kj}L)[\gamma_{kj}^2 + \rho^2\omega^2/Z_1Z_2] \tag{26}$$

$$e_{kj}^{(1)} = \rho\omega^2\gamma_{kj} \sin(\gamma_{kj}L) \tag{27a}$$

$$e_{kj}^{(2)} = \rho^2\omega^3 \cos(\gamma_{kj}L) \tag{27b}$$

$$e_{kj}^{(3)} = \rho\omega^2\gamma_{kj} \cos(\gamma_{kj}L) \tag{27c}$$

$$e_{kj}^{(4)} = \rho^2\omega^3 \sin(\gamma_{kj}L) \tag{27d}$$

$$L_{sqkj}^{L,R} = \int_0^{R^p} \int_0^{2\pi} r Y_{sq}^{L,R}(r,\theta) Y_{kj}\, dr\, d\theta; \quad R^p \le R + h_s \tag{28}$$

The modes of shell and circular end-plate vibrations, corresponding to simply supported boundary conditions, are taken to be

$$X_{mn}^s(x,\theta) = \sin(m\pi x/L) \cos(n\theta) \tag{29}$$

$$Y_{sq}^{L,R}(r,\theta) = \left[J_s(k_{sq}^{L,R} r) - J_s(k_{sq}^{L,R} R^p) \frac{I_s(k_{sq}^{L,R} r)}{I_s(k_{sq}^{L,R} R^p)} \right] \cos(s\theta); \quad R^p \le R + h_s \tag{30}$$

where $k_{sq}^{L,R} = \alpha_{sq}^{L,R}/R^p$, in which $\alpha_{sq}^{L,R}$ is the qth root of the characteristic equation of circular plate vibrations,[18] and R^p is the radius of the circular plate as shown in Fig. 1. The superscripts L and R denote the end plates at $x = 0$ and $x = L$. The generalized deflection responses $\bar{A}_{mn}^B$, $\bar{A}_{sq}^L$, and $\bar{A}_{sq}^R$ of the shell and the end plates, respectively, are discussed later. Expressions for the structural-acoustic coupling terms L_{mnij} and $L_{sqkj}^{L,R}$, for simply supported boundary conditions, are given in the Appendix.

The acoustic resonant frequencies for the cylindrical closed enclosure can be calculated from

$$J_j'(\sigma_i R) = 0 \tag{31}$$

where $\beta = 0$ is used in Eq. (15). For each combination of i,j modal indices, there are k zeros of Eq. (31). This condition then gives all of the acoustic modal frequencies ω_{ijk} of the closed cylindrical enclosure shown in Fig. 1.

The total acoustic pressure inside the shell enclosure can be calculated from Eqs. (1), (20), and (21). Assuming the input loads are stationary random processes, the spectral density of the acoustic pressure p can be obtained by taking the Fourier transform and then the mathematical expectation[25,28,29] of Eq. (1). The result is

$$S_p(x,r,\theta,\omega) = S_{p_1}(x,r,\theta,\omega) + 2S_{p_1p_2}(x,r,\theta,\omega) + S_{p_2}(x,r,\theta,\omega) \tag{32}$$

where S_{p_1}, S_{p_2}, and $S_{p_1p_2}$ are the spectral densities and the cross-spectral densities of the acoustic pressures p_1 and p_2, respectively. If the responses of the shell and plates are taken to be independent, the cross-spectral densities $S_{p_1p_2} = 0$. The spectral densities S_{p_1} and S_{p_2} are calculated from Eqs. (20) and (21) in terms of the generalized coordinates of the shell $\bar{A}_{mn}^B$ and the end plates $\bar{A}_{sq}^L$ and $\bar{A}_{sq}^R$. These generalized coordinates are functions of the prescribed random inputs acting on the shell and/or the plate surfaces. A more detailed discussion on structural response and input loads is given in the following section. Then, the sound pressure levels in the enclosure can be calculated from

$$SPL(x,r,\theta,\omega) = 10\log\left[S_p(x,r,\theta,\omega) \frac{\Delta\omega}{p_o^2} \right] \tag{33}$$

where $\Delta\omega$ is the selected frequency bandwidth, and p_o is the reference pressure ($p_o = 20\ \mu N/m^2$).

Structural Response Solution

The solutions for the acoustic pressure given in Eqs. (20) and (21) are functions of the inner shell motion w_B and the inner circular plate motions w_1 and w_2. In this analysis the shell and the end plates as shown in Fig. 1 are taken to be simply supported along the edges. The double-wall shell considered is constructed from two thin composite cylindrical shells and a soft viscoelastic core. The core material is taken to be relatively soft, so that bending and shearing stresses in the core can be neglected, and consequently the core can be characterized by a uniaxial constitutive law.[11] A linear viscoelastic model is chosen to describe the behavior of the core. Both multilayered face shells are modeled according to the theory presented in Refs. 12–17. This theory is appropriate for many layers, each arbitrarily oriented with arbitrary material properties, a general anisotropic formulation. The double-wall system of the end caps is composed of soft core and two elastic circular plates, as shown in Fig. 1. The exterior and the interior plates are simply supported on all edges. The viscoelastic core model is assumed to be similar to the one used for the double-wall shell.

The governing equations and solutions for the response of single circular plates are available.[18-20] These procedures have been extended for response analysis of double-wall circular plates excited by random loads.[26] Using these solutions, the acoustic pressure p_2 given in Eq. (21) is calculated in terms of generalized coordinates $\bar{A}_{sq}^L$ and $\bar{A}_{sq}^R$ of the inner plate motions at $x = 0$ and $x = L$. Because of very lengthy expressions of the resulting equations, the structural response solutions of the shell and end-plate vibrations are not presented in this paper. However, a detailed treatment on the response of double-wall composite shells and double-wall circular plates is given in Refs. 26 and 27.

Input Loads

The input loads are modeled either as uniformly distributed random pressures or random point loads acting at an arbitrary location of the shell surface or the end-plate surface. Point loading can be a representation of excitations that may be generated by vibrating mounting equipment and/or masses. In the vicinity of a point load some of the assumptions of linear, elastic, thin shell theory are violated.[17] However, outside the vicinity of the point load, shell response can be calculated with good accuracy. A Dirac delta function is used to define the point load. The point loads are then expressed in terms of distributed loads p^e and p^i as

$$p^e(x,\theta,t) = (1/A_1^e A_2^e)[F_1^e(t)\delta(x - x_1^e)\delta(\theta - \theta_1^e) + F_2^e(t)\delta(x - x_2^e)\delta(\theta - \theta_2^e)] \tag{34}$$

$$p^i(x,\theta,t) = (1/A_1^i A_2^i)[F_1^i(t)\delta(x - x_1^i)\delta(\theta - \theta_1^i) + F_2^i(t)\delta(x - x_2^i)\delta(\theta - \theta_2^i)] \tag{35}$$

where the superscripts e and i denote the external and the internal shells, respectively, and δ is the Dirac delta function. For a cylindrical shell $A_1^e = 1$, $A_2^e = R + h_s$, $A_1^i = 1$, and $A_2^i = R$. The location of the point loads acting on the shell surface are given in Fig. 2. The point loads are assumed to be independent, and each is characterized by a spectral density.

Numerical Results

Numerical results presented herein are for the double-wall-laminated shell system shown in Figs. 1 and 2. In the present paper most of the numerical results are presented for noise transmitted and noise generated by vibrations of the shell structure. In this case the end caps are assumed to be acoustically hard. However, preliminary results of noise transmission

by the double-wall end plates are included. The dimensions of the double-wall shell are $L = 7.62$ m, $R = 1.473$ m, and $h_s = 5.08$ cm. For the circular end plates $R^p = R$ and $h_s^p = h_s$. The thicknesses of the outer and the inner shells are $h_E = 0.813$ mm and $h_I = 2.54$ mm. The thicknesses of both end plates are selected to be the same and equal to $h_B^P = h_T^P = 6.35$ mm. The stiffness and density of core material are $k_s = 1.14 \times 10^6$ N/m^3 and $\rho_s = 37.402$ Pa-s^2/m^2. The speed of sound in the interior and the air density and flow resistivity of porous acoustic material lining of the interior surfaces are $c = 342.82$ m/s, $\rho = 1.225$ Pa-s^2/m^2, and $R_1 = 4.23 \times 10^4$ mks ryal/m, respectively. The sound pressure levels are computed at $x = L/2$, $r = 0.584$ m, and $\theta = 45$ deg. To save computation time, only one location inside the shell was selected for sound pressure calculations. The acoustic point impedance of porous materials was calculated from[26,28,29]

$$Z_A = Z_1 = Z_2 = -c\rho\{[1 + 0.0571(2\pi R_1/\omega\rho)^{0.754}] + i[0.087(2\pi R_1/\omega\rho)^{0.732}]\} \quad (36)$$

The equivalent acoustic damping parameter β due to viscous air damping and wall absorption was calculated from

$$\beta = 2\zeta^a\omega^l/c^2 \quad (37)$$

where ω^l is the lowest acoustic modal frequency in the enclosure. In using Eq. (37) the acoustic modal damping ratios are taken $\zeta_{ijk} = \zeta^a(\omega^l/\omega_{ijk})$, where ω_{ijk} are modal frequencies and ζ^a is the damping coefficient corresponding to the first lowest acoustic modal frequency in the cylindrical enclosure.

Numerical results are obtained for aluminum- and fiber-reinforced laminated double-wall shells and aluminum circular plates. The fiber orientation is prescribed by angle α (Fig. 1). The frequency range considered is 0–1000 Hz. Response and noise transmission calculations are obtained at multiple frequency values of 2 Hz. The input random pressure p^e, p^i and the point loads F_j^e, F_j^e ($j = 1, 2$) are characterized by the truncated Gaussian white noise spectral densities,

$$S_{p^e,p^i} = \begin{cases} 318\ (\text{N/m}^2)^2/\text{Hz}, & 0<f<1000\ \text{Hz} \\ 0 & \text{otherwise} \end{cases} \quad (38)$$

$$S_{Fj,Fj^e} = \begin{cases} 4.95 \times 10^{-3}\ \text{N}^2/\text{Hz}, & 0<f<1000 \\ 0 & \text{otherwise} \end{cases} \quad (39)$$

The spectral densities of the uniformly distributed random pressures p^e and p^i given in Eq. (38) correspond to a 120-dB truncated Gaussian white noise pressure. These noise levels and the magnitude of input point loads characterized by spectral densities given in Eq. (39) were selected in such a way that the resulting maximum shell or plate response is linear and equal to about one-half the value of the outer shell or outer plate thickness. For the numerical computations the same values of spectrum densities are used for the external and the internal loadings.

The first 64 acoustic resonant frequencies ω_{ijk} for the cylindrical closed enclosure were obtained by solving Eq. (31) and are given in Table 1. For the subscripts in ω_{ijk}, i is the number of axial half-waves, j is the number of nodal diameters, and $k - 1$ is the number of nodal circles. The lowest acoustic modal frequency in the enclosure is 22.56 Hz, which corresponds to the first longitudinal (x direction) in the shell.

The sound pressure levels normalized to the highest peak are presented in Fig. 3 for reverberant ($Z_A \to \infty$, $\beta = 0$) and highly absorbent conditions [Z_A given in Eq. (39), $\beta = 1.6 \times 10^{-4}$ rad-s/m^2]. In obtaining these results the following data were used: uniform random pressure acting on the exterior shell, both shells are made of aluminum with densities $\rho_E = \rho_I = 2768$ Pa-s^2/m^2, elastic moduli $E_E = E_I = 7.24 \times 10^{10}$ Pa, Poisson's ration $\nu_E = \nu_I = 0.3$, and constant structural modal damping coefficients $\zeta_o^E = \zeta_o^I = 0.03$, where the superscripts and/or subscripts E and I denote the external and internal shell, respectively. The stiffness of the core is $k = k_s(1 + ig_s)$, where the structural loss factor of the core is $g_s = 0.02$. Up to 10 structural modes are included for each of the circumferential and the longitudinal directions. However, for a uniformly distributed input of an axially symmetric shell, only the modes for which $n = 0$ are excited. As can be seen from Fig. 3, a large number of acoustic modes is excited for reverberant conditions. For highly absorbent interiors, peaks are observed only at the structural modal frequencies. The modal frequencies corresponding to the breathing mode of the flexural and dilatational motions of the double-wall structure are at 490 and

Table 1 Modal acoustic frequencies of the cylindrical enclosure

i	j	k	ω_{ijk}	i	j	k	ω_{ijk}	i	j	k	ω_{ijk}	i	j	k	ω_{ijk}
0	0	1	0.0000	1	1	2	199.4405	2	2	3	371.7686	3	3	4	544.1061
0	0	2	142.4452	1	1	3	317.8213	2	2	4	489.9615	3	4	1	209.3995
0	0	3	261.3043	1	1	4	436.4621	2	3	1	163.6457	3	4	2	349.6330
0	0	4	376.4491	1	2	1	114.9657	2	3	2	301.8392	3	4	3	474.1628
0	1	1	68.1583	1	2	2	251.1765	2	3	3	423.4321	3	4	4	595.7382
0	1	2	198.1604	1	2	3	369.7093	2	3	4	541.7625	4	0	1	90.2400
0	1	3	317.0195	1	2	4	488.4008	2	4	1	203.2323	4	0	2	168.6236
0	1	4	435.8786	1	3	1	158.9122	2	4	2	345.9747	4	0	3	276.4475
0	2	1	112.7304	1	3	2	299.2993	2	4	3	471.4717	4	0	4	387.1139
0	2	2	250.1613	1	3	3	421.6252	2	4	4	593.5985	4	1	1	113.0876
0	2	3	369.0204	1	3	4	540.3516	3	0	1	67.6800	4	1	2	217.7402
0	2	4	487.8795	1	4	1	199.4405	3	0	2	157.7061	4	1	3	329.6129
0	3	1	157.3026	1	4	2	343.7610	3	0	3	269.9269	4	1	4	445.1218
0	3	2	298.4478	1	4	3	469.8497	3	0	4	382.4847	4	2	1	144.4002
0	3	3	421.0213	1	4	4	592.3110	3	1	1	96.0528	4	2	2	265.9397
0	3	4	539.8804	2	0	1	45.1200	3	1	2	209.3995	4	2	3	379.8939
0	4	1	198.1604	2	0	2	149.4204	3	1	3	324.1635	4	2	4	496.1549
0	4	2	343.0200	2	0	3	265.1712	3	1	4	441.1017	4	3	1	181.3488
0	4	3	469.3078	2	0	4	379.1435	3	2	1	131.4866	4	3	2	311.7921
0	4	4	591.8812	2	1	1	81.7396	3	2	2	259.1549	4	3	3	430.5835
1	0	1	22.5600	2	1	2	203.2323	3	2	3	375.1755	4	3	4	547.3701
1	0	2	144.2207	2	1	3	320.2143	3	2	4	492.5515	4	4	1	217.7402
1	0	3	262.2764	2	1	4	438.2077	3	3	1	171.2446	4	4	2	354.6913
1	0	4	377.1245	2	2	1	121.4247	3	3	2	306.0256	4	4	3	477.9048
1	1	1	71.7949	2	2	2	254.1977	3	3	3	426.4264	4	4	4	598.7209

Subscript i, number of equal half-waves; subscript j, number of modal diameters; k-1, number of modal circles.

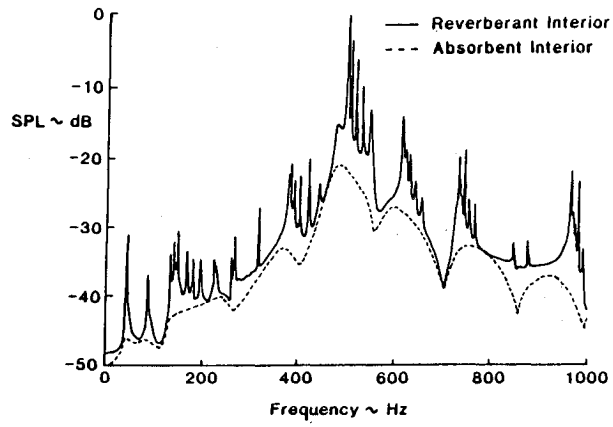

Fig. 3 Normalized sound pressure levels in a double-wall aluminum shell (under uniform exterior pressure).

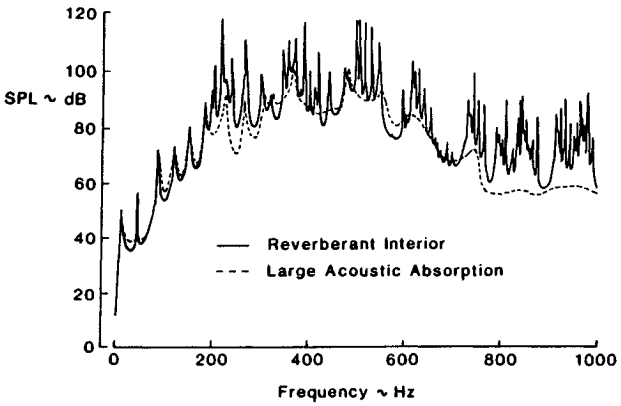

Fig. 4 Sound pressure levels of a double-wall aluminum shell (exterior point loads).

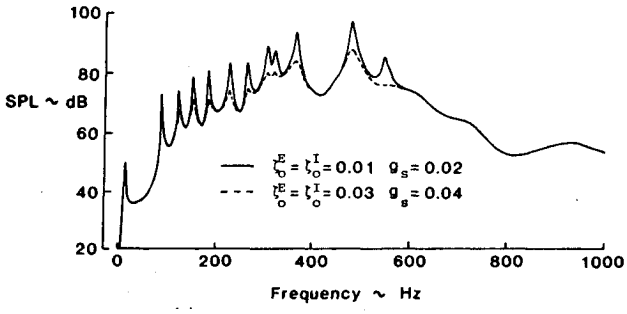

Fig. 5 Sound pressure levels in a shell for low and high structural damping values (exterior point loads).

600 Hz. Sound pressure levels at these frequencies are significantly higher compared to other response peaks.

In Fig. 4 the same shell configuration is used, but the inputs are two point loads located on the exterior shell surface $x_1^e = x_2^e = 3.81$ m, $\theta_1^e = -90$ deg, and $\theta_2^e = 90$ deg. The structural and acoustic damping parameters are $\zeta_o^E = \zeta_o^I = 0.01$ and $\beta = 1.6 \times 10^{-5}$ rad-s/m^2.

The results of Figs. 3 and 4 indicate that many more structural modes are excited for point load inputs. Even though the sound pressure levels in a shell with large acoustic absorption are dominated by the flexural breathing mode, the sound pressure levels at other structural modes excited by point loads are relatively high. The results presented in these figures clearly illustrate the difference between the noise transmitted due to a uniformly distributed acoustic pressure input and sound generated by point loads.

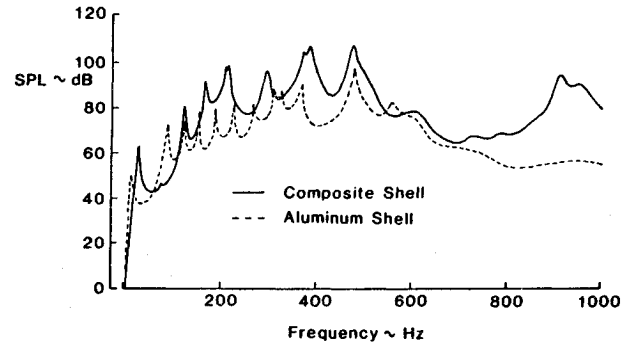

Fig. 6 Sound pressure levels for aluminum and composite shells (exterior point loads).

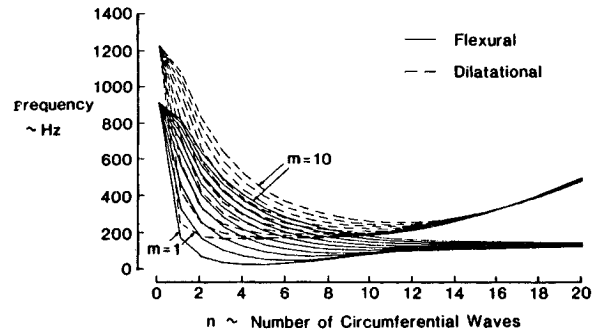

Fig. 7 Modal frequencies of a double-wall composite shell.

The results shown in Fig. 5 are for the same shell and identical point load excitation, but higher modal and core damping. It is seen from Fig. 5 that, for higher damping in the shell and the core, the sound pressure levels are significantly lower at the modal response peaks.

For the results that follow, the fiber orientation, except when stated, of the composite shell will be as follows: The outer composite shell is constructed from three layers with fiber orientation for each layer $\alpha_{1T} = -45$ deg (fiberglass fibers), $\alpha_{2T} = 45$ deg (graphite fibers), and $\alpha_{3T} = -45$ deg (fiberglass fibers). The graphite and fiberglass fibers are imbedded in a Plexiglas material with a volumetric ratio of fibers to material 0.2. The elastic moduli and material densities

are $E_{\text{fiberglass}} = 5.17 \times 10^{10}$ Pa, $E_{\text{graphite}} = 7.032 \times 10^{11}$ Pa, $E_{\text{Plexiglas}} = 1.57 \times 10^9$ Pa, $\rho_{\text{fiberglass}} = 2180$ Pa-s^2/m^2, $\rho_{\text{graphite}} = 1550$ Pa-s^2/m^2, $\rho_{\text{Plexiglas}} = 1197$ Pa-s^2/m^2. The inner shell is composed of 10 layers of Plexiglas material reinforced with graphite and fiberglass fibers. The fiber orientations for each layer are -45 deg (fiberglass fibers), 45 deg (graphite fibers), -45 deg (fiberglass fibers), etc. The mass per unit area of the composite shell is calclated from

$$m_c^s = \sum_{k=1}^{N} \rho_k (h_{k+1} - h_k) \tag{40}$$

where ρ_k and h_k are material density and thickness of the kth layer, respectively. The procedures given in Refs. 16 and 17 are used to calculate stiffness coefficients for a laminated shell.

Figure 6 depicts sound pressure levels for a double-wall aluminum shell and a double-wall-laminated fiber-reinforced shell under exterior point load inputs. The results shown in Fig. 6 correspond to $\zeta_o^E = \zeta_o^I = 0.01$, $g_s = 0.02$, and $\beta = 1.6 \times 10^{-5}$ rad-s/m^2. As can be observed from these results, the noise levels generated by the composite shell system are higher than the noise levels for the aluminum shell system at most frequencies.

For a shell structure a shift in modal frequency could induce different coupling between structural and acoustic modes. A natural frequency plot for the double wall composite shell is given in Fig. 7. Only the first 10 longitudinal modes are

included in this figure. As can be observed from these results, a large number of modes might participate at some frequencies.

The effect of structural and acoustic damping on sound generation is illustrated in Fig. 8. These results correspond to $\beta = 1.6 \times 10^{-5}$ rad-s/m^2. As can be seen from these results, a significant amount of noise reduction can be achieved in a composite shell by increasing structural and acoustic damping. A soft viscoelastic core bonded between the two shells could provide an increase in structural damping, resulting in lower interior noise levels. The results shown in Fig. 8 indicate that, for acoustically hard interior walls ($Z_A \to \infty$), the noise levels in the cylinder become relatively large.

A direct comparison of interior sound pressure levels in the cylinder excited by the exterior and interior point loads is given in Fig. 9. The loading conditions are the same for both of those cases. Since vibration coupling is provided by the viscoelastic core, the noise generated in the interior is a function of how the point loads are acting on the double-wall shell.

The results presented in Fig. 10 correspond to point loads acting on the interior shell at $x_1^i = x_2^i = 3.81$ m, $\theta_1^i = -90$ deg, and $\theta_2^i = 90$ deg. The fiber orientation for the three layers (Fig. 1) of the exterior shell is described on Fig. 10. The fiber orientations for the 10 layers of the interior shell are $[(0/22.5/45)_s/90_4]$ (A), $[90/0]_5$ (B), and $[-45/45]_5$ (C). The fiber reinforcement fiberglass/graphite pattern is repeated for all layers. These results show that shell response and interior noise are functions of fiber orientation in a composite shell. The interior noise levels might be tailored to meet specific needs by selection of a suitable fiber orientation. However, interior

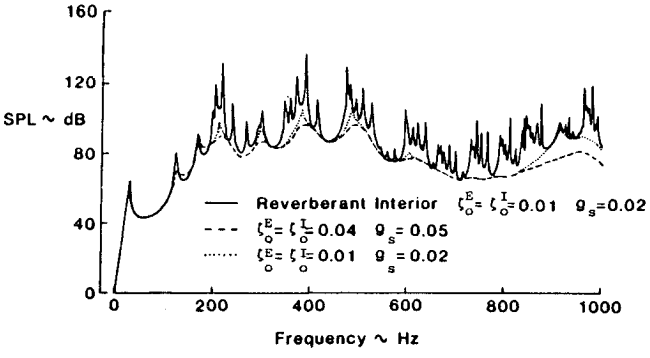

Fig. 8 Sound pressure levels for different structural and acoustic damping conditions (exterior point loads).

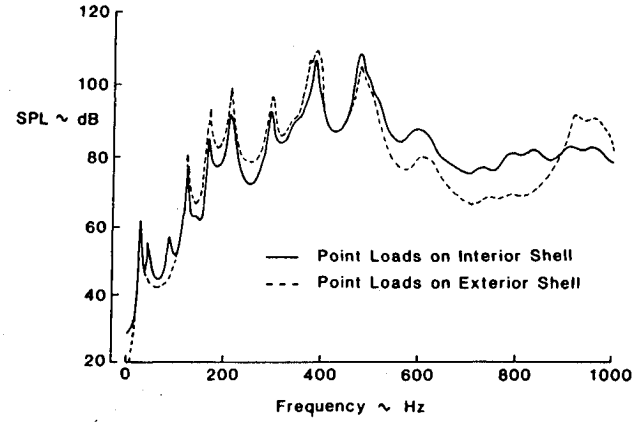

Fig. 9 Sound pressure levels in a composite shell for different point loading conditions.

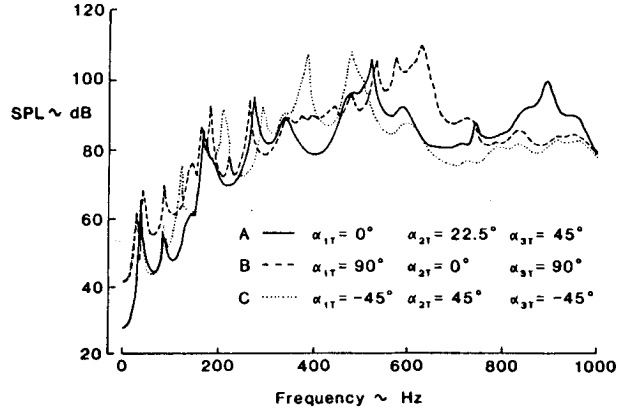

Fig. 10 Sound pressure levels in a composite shell for different fiber orientations (interior point loads).

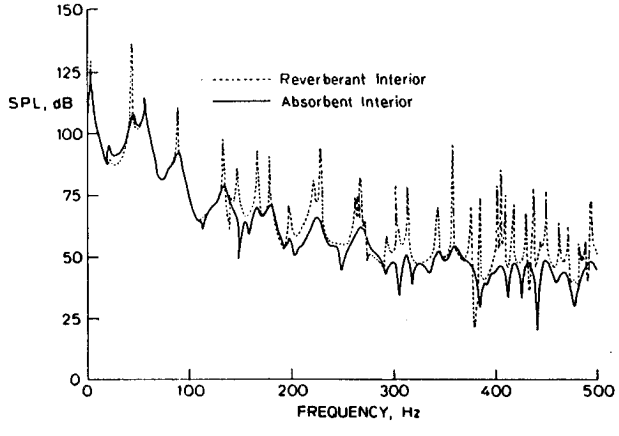

Fig. 11 Sound pressure levels due to end plates (at $x = L$) for different acoustic conditions (exterior uniform pressure).

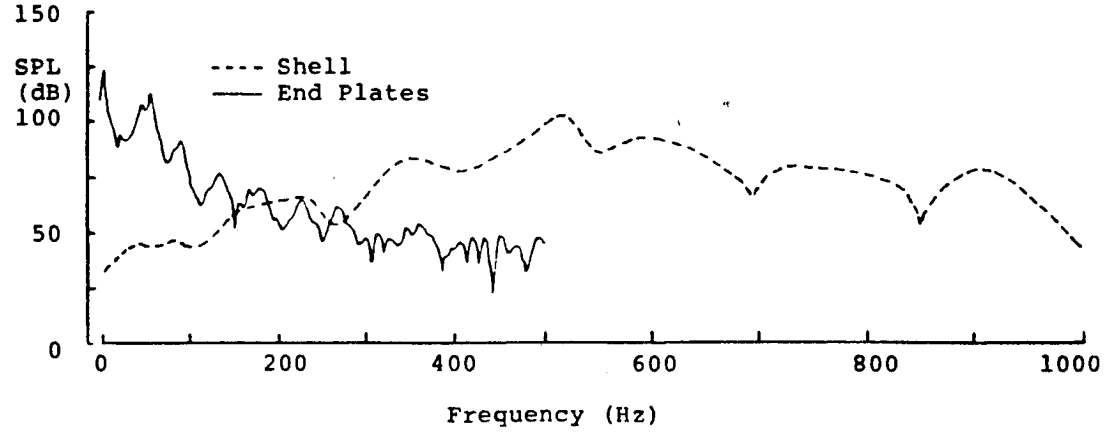

Fig. 12 Sound pressure levels due to individually vibrating shell and end-plate sytems (exterior uniform pressure).

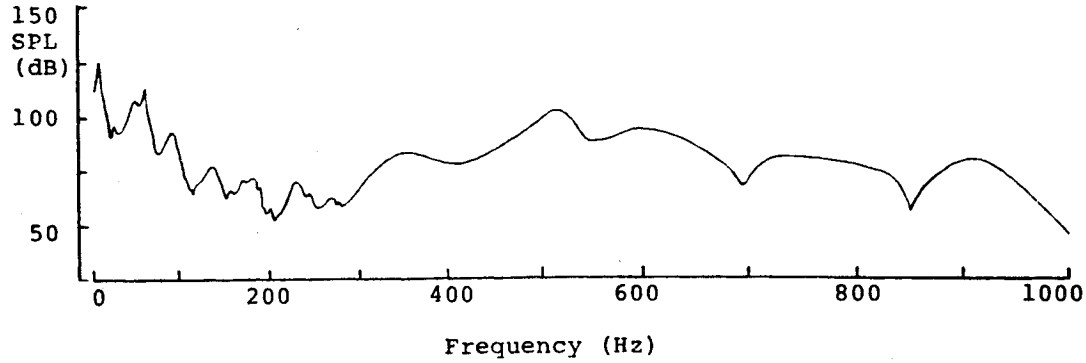

Fig. 13 Total interior noise due to exterior uniform pressure.

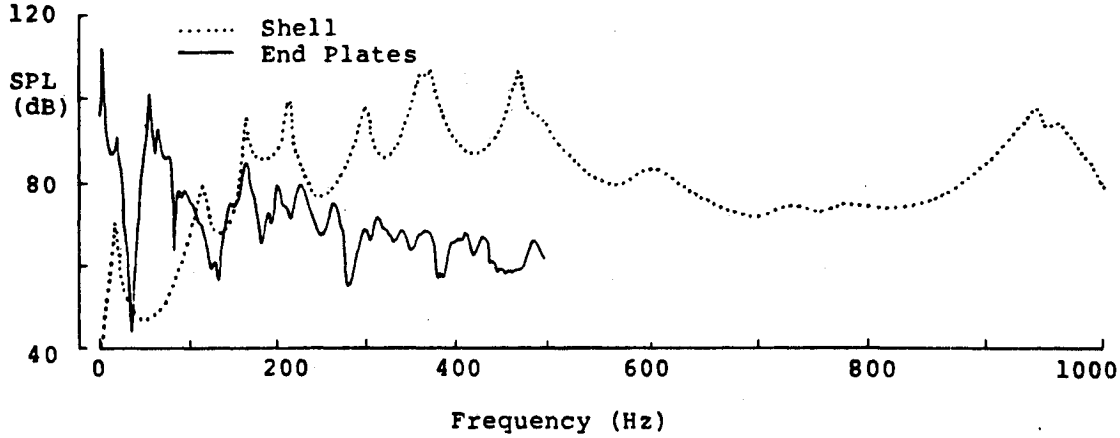

Fig. 14 Sound pressure levels due to individually vibrating shell and end-plate systems (exterior point loads).

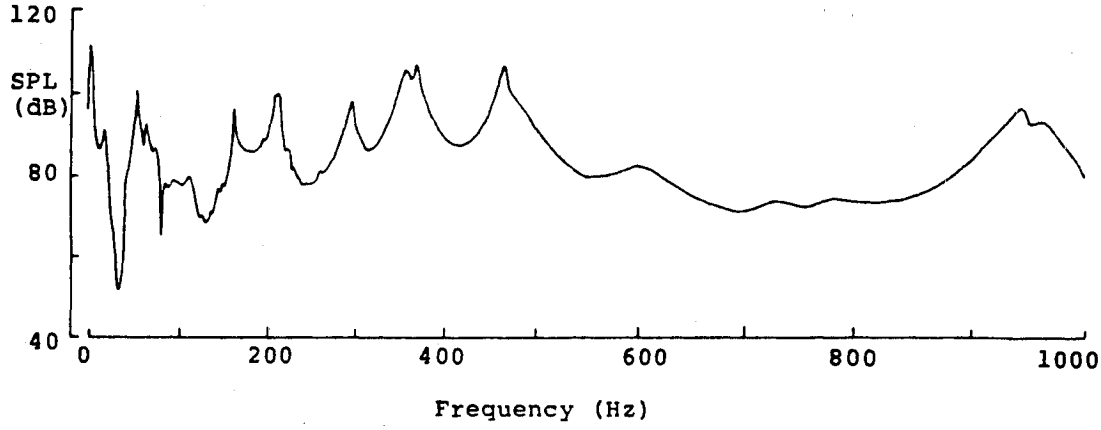

Fig. 15 Total interior noise due to exterior point loads.

noise is a function of frequency, and only specific frequency bands might be affected by this procedure.

The sound pressure levels at $x = L/2$, $r = 0.584$ m, and $\theta = 45$ deg, due to noise transmitted through double-wall aluminum circular end plates, is shown in Fig. 11 for reverberant and absorbent interiors. The input is a uniform 120-dB acoustic pressure acting on the exterior end plate, which is located at $x = L$. In this case the end plate located at $x = 0$ is assumed to be rigid. The reverberant and absorbent conditions are simulated by selecting $Z_A \to \infty$, $\beta = 0$, and Z_A as given in Eq. (39), and $\beta = 1.6 \times 10^{-4}$ rad-s/m^2, respectively. As can be seen from Fig. 11, a large number of acoustic modes are excited by the vibration of end plates for reverberant conditions. Modal plate damping is taken to be constant and equal to $\zeta_o^p = 0.06$. The structural loss factor of the core $g_s^p = 0.02$. The noise transmission by the end caps is predominantly low frequency. The fundamental circular plate frequency is 3.53 Hz and the lowest acoustic modal frequency in the shell enclosure is 22.56 Hz.

Figure 12 shows the results of noise generated inside the enclosure due to uniform random pressure applied on the exterior surfaces of the double-wall aluminum shell and double-wall aluminum end plates. It can be seen that transmitted noise is dominated by end-plate vibrations for frequencies up to 200 Hz and by shell vibrations for frequencies above 200 Hz. Because of the assumption of independently vibrating double-wall shell and end-plate systems, the total interior pressure can be calculated by a superposition of the individual contributions. Then, the total interior pressure is presented in Fig. 13. Similar results are presented in Figs. 14 and 15 for random point load inputs. These loads were applied on the exterior surfaces of the shell and end-plate systems. As can be observed from these results, low-frequency noise is dominated by end-plate motions, and neglecting noise transmitted by the

end caps could underestimate interior sound pressure levels for the low-frequency region.

Conclusions

An analytical model has been developed to predict the structure-borne noise in a double-wall cylindrical composite shell. Results indicate that interior noise is strongly dependent on the damping characteristics of the shell, the end plates and the core, the location of point load action, the acoustic absorption at the interior walls, and the fiber orientation of the different layers. A composite shell tends to generate more noise than a geometrically equivalent aluminum shell. However, by proper selection of core damping and fiber orientation, a significant amount of noise attenuation might be achieved by a design composed of two composite shells and a soft viscoelastic core.

Appendix

The structural-acoustic coupling terms are

$$L_{sqkj}^{L,R} = \begin{cases} 0, & s \neq k \\ \dfrac{\pi(R^p)^2}{(\bar{\alpha}_{kj}\xi)^2 - (\alpha_{kq}^{L,R})^2} \cdot [\alpha_{kq}^{L,R} J_k(\bar{\alpha}_{kj}\xi) J_k'(\alpha_{kq}^{L,R}) - \bar{\alpha}_{kj}\xi J_k(\alpha_{kq}^{L,R}) J_k'(\bar{\alpha}_{kj}\xi)] \\ \quad + \dfrac{\pi(R^p)^2}{(\bar{\alpha}_{kj}\xi)^2 + (\alpha_{kq}^{L,R})^2} \cdot \dfrac{J_k(\alpha_{kq}^{L,R})}{I_k(\alpha_{kq}^{L,R})} \cdot [\bar{\alpha}_{kj}\xi I_k(\alpha_{kq}^{L,R}) J_k'(\bar{\alpha}_{kj}\xi) - \alpha_{kq}^{L,R} J_k(\bar{\alpha}_{kj}\xi) I_k'(\alpha_{kq}^{L,R})], & k \neq 0 \\ \dfrac{2\pi(R^p)^2}{(\bar{\alpha}_{0j}\xi)^2 - (\alpha_{0q}^{L,R})^2} \cdot [\alpha_{0q}^{L,R} J_0(\bar{\alpha}_{0j}\xi) J_0'(\alpha_{0q}^{L,R}) - \bar{\alpha}_{0j}\xi J_0(\alpha_{0q}^{L,R}) J_0'(\bar{\alpha}_{0j}\xi)] \\ \quad + \dfrac{\pi(R^p)^2}{(\bar{\alpha}_{0j}\xi)^2 + (\alpha_{0q}^{L,R})^2} \cdot \dfrac{J_0(\alpha_{0q}^{L,R})}{I_0(\alpha_{0q}^{L,R})} \cdot [\bar{\alpha}_{0j}\xi I_0(\alpha_{0q}^{L,R}) J_0'(\bar{\alpha}_{0j}\xi) - \alpha_{0q}^{L,R} J_0(\bar{\alpha}_{0j}\xi) I_0'(\alpha_{0q}^{L,R})], & k = 0 \end{cases}$$

where $\xi = R^p/R$, and $\bar{\alpha}_{kj}$ is the jth root of the equation $dJ_k/dr = 0$, and $\alpha_{kq}^{L,R}$ is the qth root of the characteristic frequency equation for circular plate vibrations.

Also,

$$L_{mnij} = \sqrt{\frac{2}{\pi L}} \cdot \begin{cases} 0, & n \neq j \\ 0, & m = i, \quad i \neq 0, \quad n = j = 0 \\ 0, & m = i, \quad i \neq 0, \quad n = j \neq 0 \\ \dfrac{L}{m}\left[1-(-1)^m\right], & m \neq 0, \quad i = 0, \quad n = j \neq 0 \\ \dfrac{2L}{m}\left[1-(-1)^m\right], & m \neq 0, \quad i = 0, \quad n = j = 0 \\ L\left[\dfrac{1-(-1)^{m+i}}{m+i} + \dfrac{1-(-1)^{m-i}}{m-i}\right], & m \neq i, \quad i \neq 0, \quad n = j = 0 \\ \dfrac{L}{2}\left[\dfrac{1-(-1)^{m+i}}{m+i} + \dfrac{1-(-1)^{m-i}}{m-i}\right], & m \neq i, \quad i \neq 0, \quad n = j \neq 0 \end{cases}$$

Acknowledgment

C. Lyrintzis was supported in part by a grant from the San Diego State University Foundation.

References

[1]Davis, G. W., and Sakata, I. F., "Design Considerations for Composite Fuselage Structure of Commercial Transport Aircraft," NASA CR-159296, March 1981.

[2]Revell, J. D., Balena, F. J., and Koval, L. R., "Analytical Study of Interior Noise Control by Fuselage Design Techniques on High-Speed, Propeller Driven Aircraft," NASA CR-159222, July 1978.

[3]Yang, J. C. S., and Tsui, C. Y., "Optimum Design of Structures and Composite Materials in Response to Aerodynamic Noise and Noise Transmission," NASA CR-155332, Dec. 1977.

[4]Durchlaub, E. C., "Minimized Fuselage Vibrations Using Advanced Composites," 33rd Annual National Forum of the American Helicopter Society, Paper 77.33-84, Washington, DC, May 1977.

[5]Koval, L. R., "Sound Transmission into a Laminated Composite Cylindrical Shell," *Journal of Sound and Vibration,* Vol. 71, No. 4, 1980, pp. 523–530.

[6]Freudenthal, A. M., and Bieniek, M. P., "Forced Vibrations of Sandwich Structures," U.S. Air Force, WADD TR-60-307, Jan. 1961.

[7]Ford, R. D., Lord, P., and Walker, A. W., "Sound Transmission Through Sandwich Constructions," *Journal of Sound and Vibration,* Vol. 5, No. 1, 1967, pp. 9–21.

[8]Smolenski, C. P., and Krokosky, E. M., "Dilatational-Mode Sound Transmission in Sandwich Panels," *Journal of the Acoustical Society of America,* Vol. 54, No. 6, Dec. 1973, pp. 1449–1457.

[9]Dym, C. L., and Lang, M. S., "Transmission of Sound Through Sandwich Panels," *Journal of the Acoustical Society of America,* Vol. 56, No. 6, Dec. 1973, pp. 1449–1457.

[10]Vaicaitis, R., "Noise Transmission by Viscoelastic Sandwich Panels," NASA TN D-8516, Aug. 1977.

[11]Vaicaitis, R., and Hong, H. K., "Nonlinear Response of Double Wall Sandwich Panels," AIAA Paper 83-1037, May 1983.

[12]Bert, C. W., Baker, J. L., and Egle, D. M., "Free Vibration of Multilayer Anisotropic Cylindrical Shells," *Journal of Composite Materials,* Vol. 3, July 1969, pp. 480–499.

[13]Roth, B. K., and Das, Y. C., "Vibration of Layered Shells," *Journal of Sound and Vibration,* Vol. 28, No. 4, 1973, pp. 737–757.

[14]Harari, A., and Sandman, B. E., "Vibratory Response of Laminated Cylindrical Shells Embedded in an Acoustic Fluid," *Journal of the Acoustical Society of America,* Vol. 60, No. 1, July 1976, pp. 117–128.

[15]Dong, S. B., "Free Vibration of Laminated Orthotropic Cylindrical Shells," *Journal of the Acoustical Society of America,* Vol. 44, No. 6, 1968, pp. 1628–1635.

[16]Soedel, W., "Simplified Equations and Solutions for the Vibration of Orthotropic Cylindrical Shells," *Journal of Sound and Vibration,* Vol. 87, No. 4, 1983, pp. 555–566.

[17]Soedel, W., *Vibrations of Shells and Plates,* Marcel Dekker, New York, 1981.

[18]Kunukkasseril, V. X., and Swanidas, A. S. J., "Normal Modes of Elastically Connected Circular Plates," *Journal of Sound and Vibration,* Vol. 30, No. 1, 1973, pp. 99–108.

[19]Schlack, A. L., Jr., Kessel, P. G., and Dong, W. N., "Dynamic Response of Elastically Supported Circular Plates to a General Surface Load," *AIAA Journal,* Vol. 10, No. 6, 1972, pp. 733–738.

[20]Chonan, S., "Random Vibration of an Annular Plate," *Journal*

of Sound and Vibration, Vol. 78, No. 1, 1981, pp. 1–13.

[21]Dowell, E. H., "Interior Noise Studies for Single and Double-Walled Cylindrical Shells," *Journal of Aircraft,* Vol. 17, No. 9, 1980, pp. 690–699.

[22]Chang, M. T., and Vaicaitis, R., "Noise Transmission into Semi-cylindrical Enclosures Through Discretely Stiffened Curved Panels," *Journal of Sound and Vibration,* Vol. 85, No. 1, 1982, pp. 71–83.

[23]Narayanan, S., and Shanblag, R. L., "Sound Transmission Through Layered Cylindrical Shells with Applied Damping Treatment," *Journal of Sound and Vibration,* Vol. 92, No. 4, 1984, pp. 541–558.

[24]Beranek, L. L., (ed.), *Noise and Vibration Control,* McGraw-Hill, New York, 1971, pp. 245–269.

[25]Lin, Y. K., *Probabilistic Theory of Structural Dynamics,* Krieger, Huntington, NY, 1976, pp. 207–228.

[26]Bofilios, D. A., "Response and Structureborne Noise Transmission of Laminated Sandwich Cylindrical Shells," Ph.D. Dissertation, Dept. of Engineering Mechanics, Columbia Univ., New York, 1985.

[27]Bofilios, D. A., and Vaicaitis, R., "Response of Double-Wall Composite Shells to Random Point Loads," *Journal of Aircraft,* Vol. 24, No. 4, 1987, pp. 268–273.

[28]Lyrintzis, C. S., and Vaicaitis, R., "Random Response and Noise Transmission of Discretely Stiffened Composite Panels," *Journal of Aircraft,* Vol. 27, No. 2, 1990, pp. 176–184.

[29]Lyrintzis, C. S., and Bofilios, D. A., "Hygrothermal Effects on Structure-Borne Noise Transmission of Stiffened Laminated Composite Plates," *Journal of Aircraft,* Vol. 27, No. 8, 1990, pp. 722–730.